Spin Rotations Induced by an Electron Running in Closed Trajectories in Gated Semiconductor Nanodevices

S. Bednarek and B. Szafran

Faculty of Physics and Applied Computer Science, AGH University of Science and Technology, al. Mickiewicza 30, 30-059 Kraków, Poland

(Received 10 July 2008; published 21 November 2008)

A design for a quantum gate performing transformations of a single electron spin is presented. The spin rotations are performed by the electron going around the closed loops in a gated semiconductor device. We demonstrate the operation of NOT, phase-flip, and Hadamard quantum gates, i.e., the single-qubit gates which are most commonly used in the algorithms. The proposed devices employ the self-focusing effect for the electron wave packet interacting with the electron gas on the electrodes and the Rashba spin-orbit coupling. Because of the self-focusing effect, the electron moves in a compact wave packet. The spin-orbit coupling translates the spatial motion of the electron into the rotations of the spin. The device does not require microwave radiation and operates using low constant voltages. It is therefore suitable for selective single-spin rotations in larger registers.

DOI: 10.1103/PhysRevLett.101.216805 PACS numbers: 73.21.La, 03.67.Lx, 73.63.Nm

Extensive work for design and construction of quantum processing devices is underway. Proposed implementations are based on various effects and systems including photonic [1] and superconducting [2] devices, nuclear magnetic resonance [3], and ion traps [4]. In one of the approaches, the quantum bits are stored by spins of electrons confined in quantum dots [5]. Such a quantum gate can be naturally combined with a classical computer. So far, the spin setup and readout [6] as well as the spin rotations [7–9] were realized.

According to the original proposal [5], a universal quantum gate requires exchange operations between pairs of spins combined with the single-spin rotations. The latter can be performed by the Rabi oscillations in an external microwave field. For a number of reasons, selective single-spin rotations are considered more challenging to implement than the spin exchange [10]. The problem with the microwave radiation is that even at magnetic fields of the order of 10 T, the spin Zeeman energy splitting is relatively low, and the resonant wavelength is of the order of millimeters, which rather excludes fast and site-selective operations on a single spin. It was therefore suggested that a universal two-qubit gate can be achieved applying the Heisenberg coupling only: employing additional registers [10], using inhomogenous Zeeman splitting [11], or exploiting the spin-orbit coupling [12]. Experimentally, site-selective single-spin rotations were eventually demonstrated with an embedded local microwave source [8] which however requires cooling of the heat generated by the AC currents. The cooling problem is avoided when the spin rotations are induced by oscillating electric fields [9] and occur due to the spin-orbit coupling. In this Letter, we propose a device in which the single-spin operations are performed without the microwave radiation or fast voltage oscillations. The proposed device is based on spatial motion of the confined electron in the presence of the spin-orbit coupling around closed loops and requires application of low DC voltages only. Spin interference of plane waves in open quantum rings [13] was previously proposed for implementation of quantum gates [14] operating at resonant wave vectors of the scattered electron. The present proposal does not require resonant interference, and in contrast to the quantum ring devices [14] the electron after the completion of the spin transformation returns to its original position. Therefore, in our proposal, the standard gate operations change exclusively the spin part of the wave function.

We recently showed that induced quantum wires and dots [15] are formed under metal gates deposited on a planar structure containing a quantum well due to the self-focusing effect [16] for the wave function of the confined electron interacting with the electron gas in the metal. This effect assists in the 100% guaranteed transfer of a stable electron packet following a trajectory which is controlled by the gate setup and applied DC voltages.

We consider a planar nanostructure of Fig. 1 with a quantum well and electrodes on top. A single electron is confined in the quantum well. We assume that the quantum well is made of a semiconductor of the diamond lattice structure (Si, Ge), in which the Dresselhaus spin-orbit

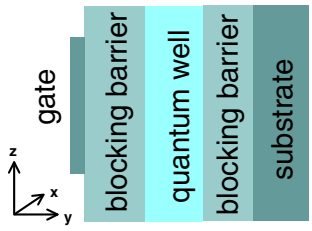

FIG. 1 (color online). The considered structure.

coupling is absent due to the inversion symmetry of the crystal. The electron motion in the y direction is frozen by the quantum well confinement. We use a two-dimensional Hamiltonian

$$H(x, z, t) = -\frac{\hbar^2}{2m}\left(\frac{\partial^2}{\partial x^2} + \frac{\partial^2}{\partial z^2}\right) - e\phi_2(x, y_0, z, t) + H_R, \tag{1}$$

where y_0 is the coordinate of the center of the quantum well and H_R is the Rashba spin-orbit coupling term due to the asymmetry of the quantum well potential $H_R = \alpha(p_z\sigma_x - p_x\sigma_z)$, where p are the momentum operators and σ's are the Pauli matrices. We write the state functions as vectors (spinors)

$$\Psi(x, z, t) = \begin{pmatrix} \psi_1(x, z, t) \\ \psi_2(x, z, t) \end{pmatrix}. \tag{2}$$

The electrostatic potential ϕ_2 of Eq. (1) is found from the Poisson equation using the methodology previously applied for simulations of electrostatic quantum dots [17]. ϕ_2 is the difference of the total electrostatic potential Φ and the electron self-interaction potential ϕ_1, $\phi_2(\mathbf{r}, t) = \Phi(\mathbf{r}, t) - \phi_1(\mathbf{r}, t)$. The total potential fulfills the 3D Poisson equation

$$\nabla^2\Phi(\mathbf{r}, t) = -\rho(\mathbf{r}, t)/\epsilon\epsilon_0, \tag{3}$$

and the self-interaction potential is calculated with the Coulomb law

$$\phi_1(\mathbf{r}, t) = \frac{1}{4\pi\epsilon\epsilon_0}\int d\mathbf{r}'\frac{\rho(\mathbf{r}', t)}{|\mathbf{r} - \mathbf{r}'|}, \tag{4}$$

where $\rho(\mathbf{r}, t)$ is the electron density calculated for wave function (2)

$$\rho(\mathbf{r}, t) = -e[|\psi_1(x, z, t)|^2 + |\psi_2(x, z, t)|^2]\delta(y - y_0). \tag{5}$$

Equation (3) is solved numerically in a rectangular box containing the studied nanostructure. Potentials applied to the gates are assumed as Dirichlet boundary condition. The content of the computational box is charge neutral, so on its surface we assume vanishing normal component of the electric field. Calculated potential $\phi_2(\mathbf{r}, t)$ contains a contribution of the charge induced on the metal surface by the confined electron. This contribution introduces the self-focusing effect [16]. The time dependence in (3–5) enters due to the motion of the electron packet. As the initial condition, we take the solution of a time-independent Schrödinger equation $H(x, z)\Psi_0(x, z) = E\Psi_0(x, z)$ for a given spin state. The time evolution is obtained numerically with a finite-difference scheme consistent with the time-dependent Schrödinger equation $\Psi(t + dt) = \Psi(t - dt) - \frac{2i}{\hbar}H(t)\Psi(t)dt$.

Applying weak voltages to the gates with respect to the substrate, one can [15] set the electron packet in motion and stop it in a chosen location. The products of the momentum and spin operators in the H_R operator perturb somewhat the electron trajectories. Electron motion influences the spin in a much more pronounced extent.

Let us consider the system presented in Fig. 2(a) with two electrodes e_1 and e_2 placed on top of the structure of Fig. 1. In the initial state, we put zero voltage to electrode e_1 and small negative to e_2 [15]. The electron localized ground state is formed under e_1. We assume that the spin is in the state which has the same average value in all x, y, z directions,

$$\Psi(x, z, 0) = \Psi_0(x, z)\frac{1}{\sqrt{2}\sqrt{\sqrt{3} + 3}}\begin{bmatrix} (1 + \sqrt{3}) \\ (1 + i) \end{bmatrix}.$$

The motion of the packet starts when the voltage applied to e_2 is switched to $V_2 = 0.2$ mV which extracts the electron from underneath the gate e_1. The time dependence of the electron position is given in Fig. 2(b) with a solid black line. The dashed curves show the average values of the components of the spin. For the electron moving parallel to the z axis, the $\langle\sigma_x\rangle$ value is preserved and the $\langle\sigma_y\rangle$ and $\langle\sigma_z\rangle$ components oscillate: the spin is rotated around the x axis. The rotation angle depends on the coupling constants, the electron effective mass, and the distance traveled by the electron. For simulations presented in Fig. 3, we assume the coupling constant $\alpha = 7.2 \times 10^{-13}$ eV m within the range predicted for the asymmetric quantum wells [18]. The quantum well and the potential barriers are taken 10 nm thick. We apply the Si material parameters $m = 0.19m_0$ and $\epsilon = 13$. We deduce that the distance for which the initial spin is restored is $\lambda_{SO} = 1.8$ μm.

Since the electron motion along perpendicular directions induces spin rotations around perpendicular axes, one can perform any rotation by making the electron move under electrodes forming a closed loop. In Fig. 3, we propose a setup performing the logical NOT operation. The electrodes are marked with the gray color. The spin of the electron

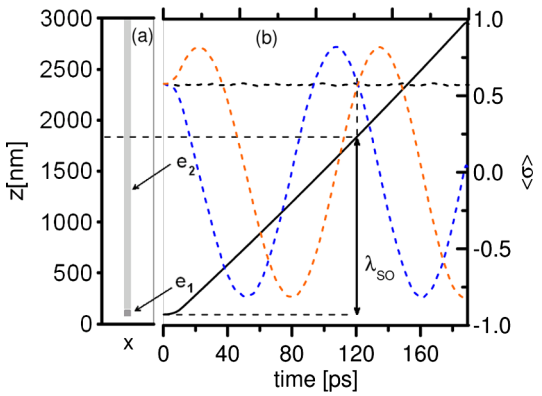

FIG. 2 (color online). (a) Position of the electrodes e_1, e_2 (arrows) on top of the structure. (b) Electron packet z position vs time (solid line, left axis). Average values (dashed lines) of the Pauli operators: $\langle\sigma_z\rangle$ [red (light gray) color], $\langle\sigma_x\rangle$ (black) and $\langle\sigma_y\rangle$ [blue (dark gray)]—referred to the right axis.

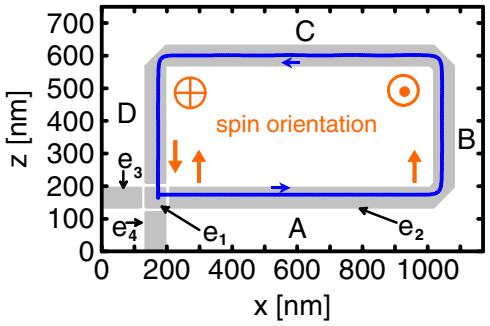

FIG. 3 (color online). Gate configuration (gray colors) for the NOT gate. Blue (dark gray) solid lines show the electron trajectory (electron starts from under e_1 and goes to the right). Red (light gray) symbols show the spin orientation near the corners of the trajectory (⊙, ⊕ indicate "from the page" and "to the page" directions, respectively).

confined in the quantum dot induced [15] under e_1 electrode stores the qubit. The e_2 electrode serves to guide the electron around a closed loop back to the dot induced under e_1. For illustration, initially the z-component of the spin is set in the "up" state

$$\Psi(x, z, 0) = \begin{pmatrix} \Psi_0(x, z) \\ 0 \end{pmatrix}.$$

The packet is set in motion to the right by applying a constant $+0.2$ mV voltage to e_2 and a short pulse of -0.4 mV to e_3. The electron trajectory is drawn with the blue (dark gray) curve in Fig. 3. The time dependence of the electron position is plotted in Fig. 4. In the A region, we notice an initial increase of the velocity and then a constant velocity motion till the end of the A segment. After reflection at the cut corner [15], the electron goes into the B part where the x position becomes fixed and the z one increases with time. Passing under the C and D segments, the electron returns to its initial position. At the end of the loop, the electron slows down which results in the e_1, e_2 potential difference. When the electron comes to under e_1, the potential of this electrode is changed to $+0.3$ meV which traps the electron in the induced dot. The oscillations of the blue (dark gray) curve at the end of the motion are due to an excess of the kinetic energy.

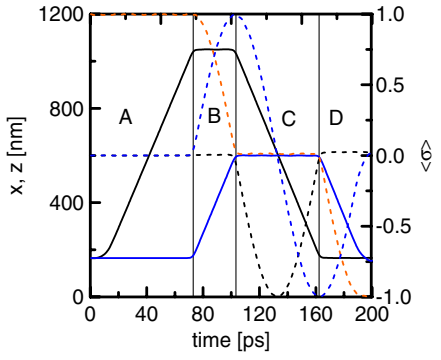

FIG. 4 (color online). Same as Fig. 2 but for the NOT gate of Fig. 3. The black [blue (dark gray)] solid curves show the x, (z) positions.

The spin direction at the corners of the loop is schematically marked by arrows in Fig. 3. The time dependence of $\langle\sigma_x\rangle$, $\langle\sigma_y\rangle$, and $\langle\sigma_z\rangle$ are plotted in Fig. 4 with dashed lines: black, blue (dark gray), and red (light gray), respectively. Initially the spin is oriented "up" $\langle\sigma_z\rangle = 1$, and $\langle\sigma_x\rangle = \langle\sigma_y\rangle = 0$. In the A segment, the electron moves in the x direction so the spin is rotated around the z axis, and no spin change is observed in Fig. 4. The length of the B segment is such that the spin is rotated around the z axis by 90° and takes the "from the page" orientation: the spin is in the σ_y eigenstate and $\langle\sigma_y\rangle = 1$. When the electron returns in the $-x$ direction, the spin is rotated by 180° and takes the "to the page" orientation $\langle\sigma_y\rangle = -1$ at the end of the C part. On the D segment, the spin is rotated by $-90°$ around the x axis. Returning to e_1, the electron is in the "down" spin eigenstate $\langle\sigma_z\rangle = -1$. Similarly one can show that the same trajectory inverts the spin of initial "down" orientation. Thus, the motion around the loop performs the NOT operation

$$U^{\text{NOT}} = \begin{pmatrix} 0 & 1 \\ 1 & 0 \end{pmatrix}. \tag{6}$$

Other useful single qubit operations are the Hadamard transformation U^H of the basis states into their equilibrated superpositions and the phase flip operation U^π

$$U^H = \frac{1}{\sqrt{2}}\begin{pmatrix} 1 & 1 \\ 1 & -1 \end{pmatrix}, \qquad U^\pi = \frac{1}{\sqrt{2}}\begin{pmatrix} 1 & 0 \\ 0 & -1 \end{pmatrix}. \tag{7}$$

The loop of Fig. 3 can be used as the Hadamard gate for the spin "up" and "down" states redefined with respect to the

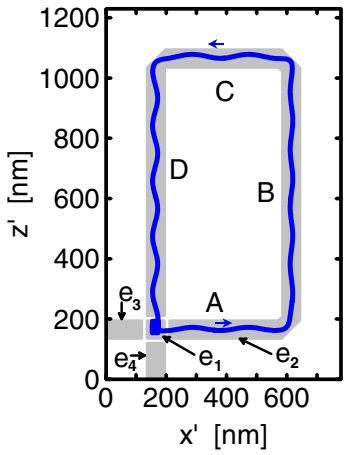

FIG. 5 (color online). Gate configuration (grey colors) for the Hadamard gate. Blue (dark gray) solid lines show the electron trajectory [electron starts from under e_1 and goes to the right—the direction of motion is marked with the blue (dark gray) arrows]. The rectangular gate path is rotated by 45° with respect to Fig. 3: $z' = \frac{1}{\sqrt{2}}(x + z)$, $x' = \frac{1}{\sqrt{2}}(x - z)$.

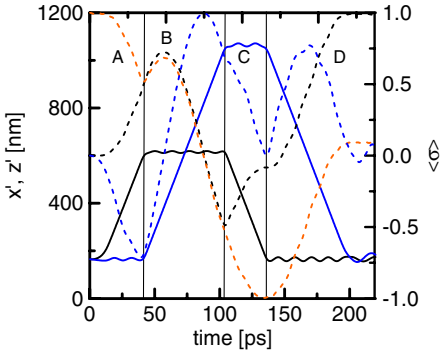

FIG. 6 (color online). Position of the electron packet as a function of time for the Hadamard gate of Fig. 5 in the rotated system of coordinates (x', y', z'). The black [blue (dark gray)] solid curves show the x', (z') positions. The dashed curve show the expectation value of the Pauli matrix operators defined with respect to the x, y, z axes.

direction bisecting the angle between x and $-z$ axes. Alternatively, one can keep the basis set and rotate the electron trajectory (the electrode loop) by 45° in the (x, y) plane. The electron trajectory in the Hadamard gate is plotted in Fig. 5 in rotated coordinate system $z' = \frac{1}{\sqrt{2}} \times (x + z)$, $x' = \frac{1}{\sqrt{2}}(x - z)$. As the initial condition for the Hadamard gate simulation, we took the electron confined below the e_1 electrode in the ground-state with the spin parallel to the z axis. The packet is set in motion to the right by introducing a potential difference between e_1 and e_2 equal to -0.2 mV. Figure 6 shows the time dependence of the spin average values. The spin initially oriented "up" $\langle \sigma_z \rangle = 1$, after closing the trajectory loop is set to the "right" $\langle \sigma_x \rangle = 1$. Similarly, the spin "down" $\langle \sigma_z \rangle = -1$ turns to the "left" at the end of the loop. Twofold rotation around the loop is equivalent to the identity transform, i.e., the rotation by the full angle.

The phase-shift operation U^{π} is performed by the electrode configuration rotated by a 90° angle with respect to the NOT gate of Fig. 3. The NOT quantum gate oriented as in Fig. 3 performs the U^{π} transformation for the "up" and "down" states redefined as parallel and antiparallel to the x axis.

The spin rotation angle is proportional to the distance traveled by the electron. In the presented simulations, the side lengths of the rectangle formed by the electrodes was set equal to λ_{SO} or $\lambda_{SO}/2$. Deviation of the length of the segments of the ideal values will decrease the probability of the operation below 1. However, the λ_{SO} values can be experimentally calibrated by tuning the Rashba coupling constant with the applied voltages. The proposed device runs on a single-electron and does not require the presence of dopants whose strong inhomogeneous field may locally perturb the spin-orbit coupling constant [19]. The devices proposed here use homogenous Rashba coupling in the absence of the Dresselhaus interaction. For devices based on zinc blende materials, one can still design electron trajectories performing the spin operations for both couplings present [20]. The dielectric constant in the nanoscale devices may have a different value than in bulk materials. However, the value of the constant affects only the strength of the self-focusing effect and not the spin rotations.

We demonstrated that the controlled electron motion around closed loops along induced quantum wires combined with the spin-orbit coupling can be used to design devices performing any single-spin rotation. The proposed device is scalable, and since it runs without a microwave radiation or high frequency electric fields, it offers an independent control of many separate qubits.

[1] J. L. O'Brien *et al.*, Nature (London) **426**, 264 (2003).
[2] Y. Nakamura, Yu. A. Pashkin, and J. S. Tsai, Nature (London) **398**, 786 (1999).
[3] L. M. K. Vandersypen *et al.*, Nature (London) **414**, 883 (2001).
[4] D. J. Wineland *et al.*, J. Res. Natl. Inst. Stand. Technol. **103**, 259 (1998).
[5] D. Loss and D. P. DiVincenzo, Phys. Rev. A **57**, 120 (1998); D. Awshalom, D. Loss, and N. Samarth, *Semiconductor Spintronics and Quantum Computation* (Springer Verlag, Berlin, 2002); R. Hanson *et al.*, Rev. Mod. Phys. **79**, 1217 (2007).
[6] J. M. Elzermann *et al.*, Nature (London) **430**, 431 (2004); R. Hanson *et al.*, Phys. Rev. Lett. **94**, 196802 (2005); T. Meunier *et al.*, Phys. Rev. B **74**, 195303 (2006).
[7] J. R. Petta *et al.*, Science **309**, 2180 (2005); F. H. L. Koppens *et al.*, Nature (London) **442**, 766 (2006); W. A. Colsh and D. Loss, Phys. Rev. B **75**, 161302 (2007).
[8] F. H. L. Koppens *et al.*, Nature (London) **442**, 766 (2006).
[9] K. C. Nowack *et al.*, Science **318**, 1430 (2007).
[10] D. P. DiVincenzo *et al.*, Nature (London) **408**, 339 (2000).
[11] J. Levy, Phys. Rev. Lett. **89**, 147902 (2002).
[12] D. Stepanenko and N. E. Bonesteel, Phys. Rev. Lett. **93**, 140501 (2004).
[13] D. Frustaglia and K. Richter, Phys. Rev. B **69**, 235310 (2004).
[14] P. Foldi, B. Molnar, M. G. Benedict, and F. M. Peeters, Phys. Rev. B **71**, 033309 (2005).
[15] S. Bednarek, B. Szafran, R. J. Dudek, and K. Lis, Phys. Rev. Lett. **100**, 126805 (2008).
[16] S. Bednarek, B. Szafran, and K. Lis, Phys. Rev. B **72**, 075319 (2005); S. Bednarek and B. Szafran, Phys. Rev. B **73**, 155318 (2006).
[17] S. Bednarek, B. Szafran, and J. Adamowski, Phys. Rev. B **61**, 4461 (2000); **64**, 195303 (2001); S. Bednarek, B. Szafran, K. Lis, and J. Adamowski, Phys. Rev. B **68**, 155333 (2003); S. Bednarek, K. Lis, and B. Szafran, Phys. Rev. B **77**, 115320 (2008).
[18] E. A. de Andrada e Silva, G. C. La Rocca, and F. Bassani, Phys. Rev. B **55**, 16293 (1997).
[19] E. Ya. Sherman, Appl. Phys. Lett. **82**, 209 (2003).
[20] S. Bednarek (to be published).